

# SCIENTIFIC REPORTS

OPEN

## Na-rich layered $\text{Na}_2\text{Ti}_{1-x}\text{Cr}_x\text{O}_{3-x/2}$ ( $x = 0, 0.06$ ): Na-ion battery cathode materials with high capacity and long cycle life

Shufeng Song<sup>1</sup>, Masashi Kotobuki<sup>2</sup>, Yingqian Chen<sup>2</sup>, Sergei Manzhos<sup>2</sup>, Chaohe Xu<sup>1</sup>, Ning Hu<sup>1,3</sup> & Li Lu<sup>2,4</sup>

Rechargeable lithium batteries have been well-known and indispensable for portable electronic devices, and have the potential to be used in electric vehicles and smart grids. However, the growing concerns about the availability of lithium resources for large-scale applications have revived interest in sodium ion batteries. Of many obstacles to commercialization of Na-ion batteries, achieving simultaneously a large reversible capacity and good cycling capability of electrode materials remains a major challenge. Here, we report a new cathode material, Na-rich layered oxide  $\text{Na}_2\text{Ti}_{0.94}\text{Cr}_{0.06}\text{O}_{2.97}$ , that delivers high reversible capacity of  $336 \text{ mAh g}^{-1}$  at current density of  $18.9 \text{ mA g}^{-1}$  along with promising cycling capability of 74% capacity retention over 1000 cycles at current of  $378 \text{ mA g}^{-1}$ . The high capacity is associated to the redox reaction of oxygen, which is confirmed here by a combined experimental and theoretical study. The present work therefore shows that materials beyond mainstream layered oxides and polyanion compounds should be considered as candidate high-performance cathodes for Na-ion batteries.

Lithium ion batteries have become an indispensable energy storage technology for mobile electronics since their commercialization, and have promise for electric vehicles as well as stationary grid applications. Nonetheless, concerns about the availability of lithium resource, which is not considered as an abundant element owing to its highly non-uniform spread within the crust of the Earth<sup>1</sup>, the significant increase of the price of lithium carbonate during the past decade, the emerging need for inexpensive stationary energy storage, all argue for research on alternatives to lithium ion batteries and arouse the research on sodium ion batteries<sup>2</sup>. In contrast to lithium, the sodium resource is evenly distributed in the Earth's crust and sodium is one of the most abundant elements with a very low material cost. In addition, sodium is the second-lightest alkali element after lithium. Moreover, sodium possesses a low redox potential ( $-2.71 \text{ V}$  vs S.H.E.), and similar electrochemistry to lithium. In view of these considerations, sodium ion batteries are the ideal alternatives to lithium ion batteries, in particular, for the stationary energy storage applications<sup>3</sup>.

Inspired by known lithium cathode materials, extensive works on sodium cathodes have been focused on conventional two-dimensional layered oxides  $\text{Na}_x\text{MO}_2$  ( $0 < x < 1$ , M: electrochemically-active transition metal) and three-dimensional polyanion compounds due to their ability to accommodate the large ionic radius and atomic weight of sodium<sup>4</sup>. Historically, the intercalation chemistry of layered sodium oxides was first investigated, which exhibited poor electrochemical performance<sup>5</sup>. The layered sodium oxides are generally composed of O3 and P2 phases depending on the coordination environment for sodium and the number of stacking transition-metal layers. O3-type  $\alpha\text{-NaFeO}_2$  (ref. 6),  $\text{NaCrO}_2$  (ref. 7),  $\text{NaNiO}_2$  (ref. 8), etc. all proved to be electrochemically active, but delivered capacities of less  $120 \text{ mAh g}^{-1}$ , corresponding to only  $\sim 0.5 \text{ Na}$  or less cycled per formula unit. Yabuuchi *et al.*<sup>9</sup> reported P2-type  $\text{Na}_{2/3}\text{Fe}_{1/2}\text{Mn}_{1/2}\text{O}_2$  that delivered an exceptionally

<sup>1</sup>College of Aerospace Engineering, Chongqing University, Chongqing, 400044, P.R. China. <sup>2</sup>Materials Science Group, Department of Mechanical Engineering, National University of Singapore, Singapore, 117575, Singapore. <sup>3</sup>The State Key Laboratory of Mechanical Transmissions, Chongqing University, Chongqing, 400044, P.R. China. <sup>4</sup>National University of Singapore Suzhou Research Institute, Suzhou, P.R. China. Correspondence and requests for materials should be addressed to S.S. (email: [sfsong@cqu.edu.cn](mailto:sfsong@cqu.edu.cn)) or N.H. (email: [ninghu@cqu.edu.cn](mailto:ninghu@cqu.edu.cn)) or L.L. (email: [luli@nus.edu.sg](mailto:luli@nus.edu.sg))

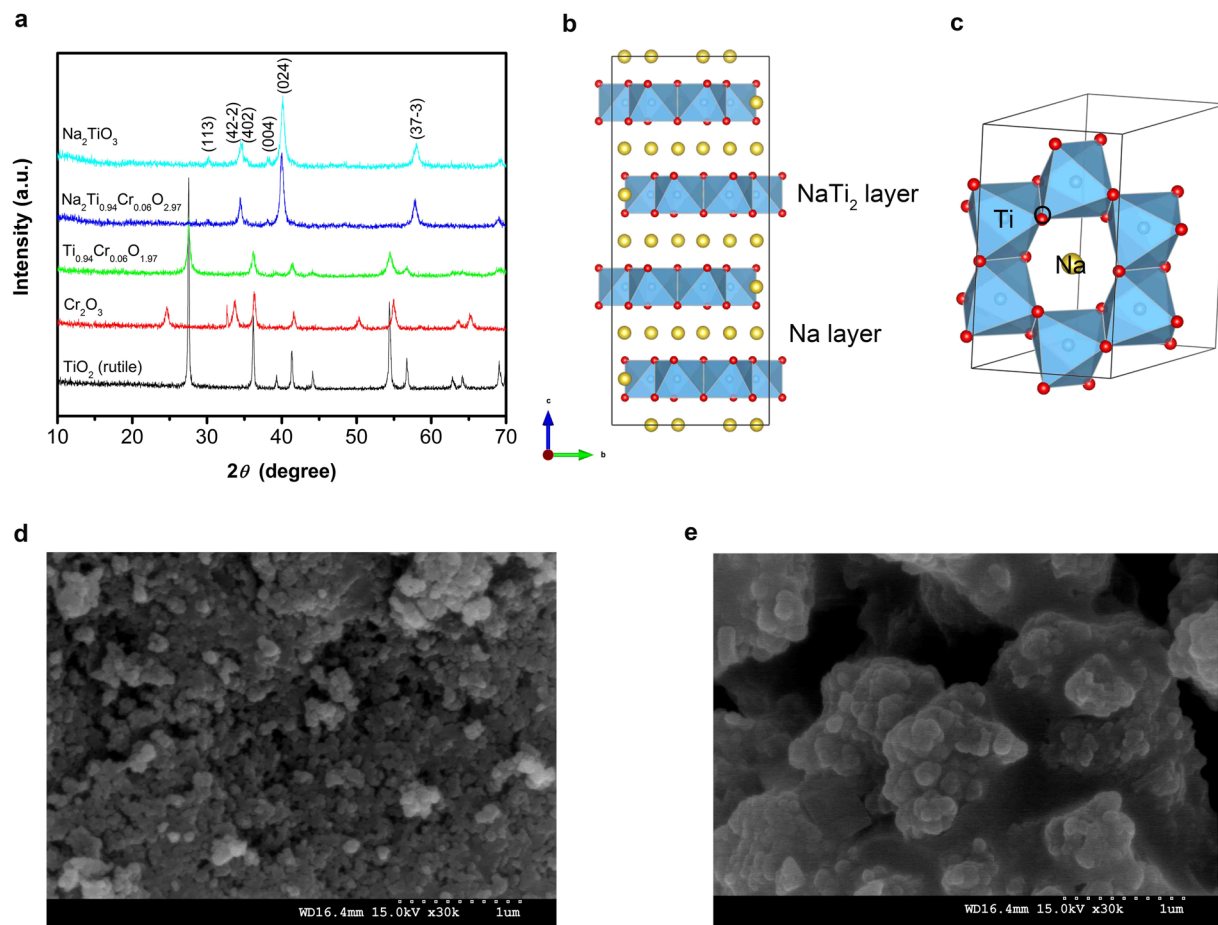


**Figure 1.** Material characterization of  $\text{Na}_2\text{TiO}_3$  and  $\text{Na}_2\text{Ti}_{0.94}\text{Cr}_{0.06}\text{O}_{2.97}$  synthesized at  $500^\circ\text{C}$  for 6 h. **(a)** XRD patterns for raw materials  $\text{TiO}_2$ ,  $\text{Cr}_2\text{O}_3$ ,  $\text{TiO}_2$ - $\text{Cr}_2\text{O}_3$  solid solution,  $\text{Na}_2\text{TiO}_3$  and  $\text{Na}_2\text{Ti}_{0.94}\text{Cr}_{0.06}\text{O}_{2.97}$ . **(b)** Crystal structure of  $\text{Na}_2\text{TiO}_3$ . **(c)** Polyhedral drawing of  $\text{Na}_{1/3}\text{Ti}_{2/3}$  layers. SEM images of as-prepared  $\text{Na}_2\text{TiO}_3$  **(d)** and  $\text{Na}_2\text{Ti}_{0.94}\text{Cr}_{0.06}\text{O}_{2.97}$  **(e)**.

high capacity of  $\sim 190 \text{ mAh g}^{-1}$  with the  $\text{Fe}^{3+}/\text{Fe}^{4+}$  redox, but its cyclability was insufficient, with the reversible capacity reduced from  $190 \text{ mAh g}^{-1}$  to  $150 \text{ mAh g}^{-1}$  after 30 cycles. Similarly, monoclinic-phase  $\alpha$ - $\text{NaMnO}_2$  (ref. 10), orthorhombic-phase  $\beta$ - $\text{NaMnO}_2$  (ref. 11), P2-type Mg-doped  $\text{Na}_{0.67}\text{Mn}_{0.8}\text{Mg}_{0.2}\text{O}_2$  (ref. 12) and so on exhibited large capacities of  $150\text{--}190 \text{ mAh g}^{-1}$ , but inferior cycle life. Johnson *et al.* (ref. 13) designed a Li-substituted layered P2-O3 intergrowth  $\text{Na}_{1-x}\text{Li}_x\text{Ni}_{0.5}\text{Mn}_{0.5}\text{O}_{2+d}$ , and Zhou *et al.* (ref. 14) reported a layered P2-O3  $\text{Na}_{0.66}\text{Li}_{0.18}\text{Mn}_{0.71}\text{Ni}_{0.21}\text{Co}_{0.08}\text{O}_{2+\delta}$  composite, that delivered a high capacity as well as better cyclability; in particular, for  $\text{Na}_{0.66}\text{Li}_{0.18}\text{Mn}_{0.71}\text{Ni}_{0.21}\text{Co}_{0.08}\text{O}_{2+\delta}$ , a good capacity retention of 75% is obtained after 150 cycles at a  $0.5 \text{ C}$  rate (ca.  $113 \text{ mAh g}^{-1}$  vs initial  $150 \text{ mAh g}^{-1}$ ). It is unsurprising that major efforts have been devoted to the research on layered sodium oxides  $\text{Na}_x\text{MO}_2$  owing to the huge commercial success of layered lithium oxides. However, a long cycle life is one of the major obstacles, and capacities must be improved further. On the other hand, the polyanion compounds possess superior cycling performance due to a strong covalent three-dimensional framework. For example, the NASICON-type  $\text{Na}_3\text{V}_2(\text{PO}_4)_3$  delivered a capacity retention of 68% after 2000 cycles at a  $5 \text{ C}$  rate, achieved by confining carbon-coated  $\text{Na}_3\text{V}_2(\text{PO}_4)_3$  nanoparticles in ordered mesoporous carbon<sup>15</sup>. However, the polyanion compounds generally suffer from low reversible capacities, due to the limited active sodium content and large molecular weight thus low theoretical capacities. For example, the initial capacities of typical polyanion cathodes  $\text{Na}_3\text{V}_2(\text{PO}_4)_3$ <sup>15</sup>, maricite-type  $\text{NaFePO}_4$ <sup>16</sup>,  $\text{Na}_{3.32}\text{Fe}_{2.34}(\text{P}_2\text{O}_7)_2$ <sup>17</sup>, and so on, were  $\sim 114$ ,  $142$ , and  $85 \text{ mAh g}^{-1}$ , respectively, corresponding to the respective theoretical capacities of  $118$ ,  $155$ , and  $118 \text{ mAh g}^{-1}$ . Therefore, it is urgent to explore cathode materials which combine high capacities (reversible and theoretical capacities) and long cycle life. Here, we report a new class of sodium cathodes,  $\text{Na}_2\text{TiO}_3$  and  $\text{Na}_2\text{Ti}_{0.94}\text{Cr}_{0.06}\text{O}_{2.97}$ , combining a high capacity  $\sim 336 \text{ mAh g}^{-1}$  and a long cycle life as well as low material cost.

## Results

**Characterization of  $\text{Na}_2\text{TiO}_3$  and  $\text{Na}_2\text{Ti}_{0.94}\text{Cr}_{0.06}\text{O}_{2.97}$ .**  $\text{Na}_2\text{TiO}_3$  and  $\text{Na}_2\text{Ti}_{0.94}\text{Cr}_{0.06}\text{O}_{2.97}$  are synthesized *via* a solid-state reaction at  $500^\circ\text{C}$  for 6 h in air. To prepare  $\text{Na}_2\text{Ti}_{0.94}\text{Cr}_{0.06}\text{O}_{2.97}$ ,  $\text{TiO}_2$ - $\text{Cr}_2\text{O}_3$  solid solution is first synthesized as precursor by high-energy ball-milling for 5 h. As shown in Fig. 1a, the  $\text{TiO}_2$ - $\text{Cr}_2\text{O}_3$  solid solution exhibits reflections of rutile-phase  $\text{TiO}_2$ , no  $\text{Cr}_2\text{O}_3$  phase is present.  $\text{Na}_2\text{TiO}_3$  has phases of  $\alpha$ ,  $\beta$  and  $\gamma$ , which exhibit face-centered cubic, monoclinic and monoclinic structures, respectively<sup>18,19</sup>. As seen in Fig. 1a,  $\text{Na}_2\text{TiO}_3$

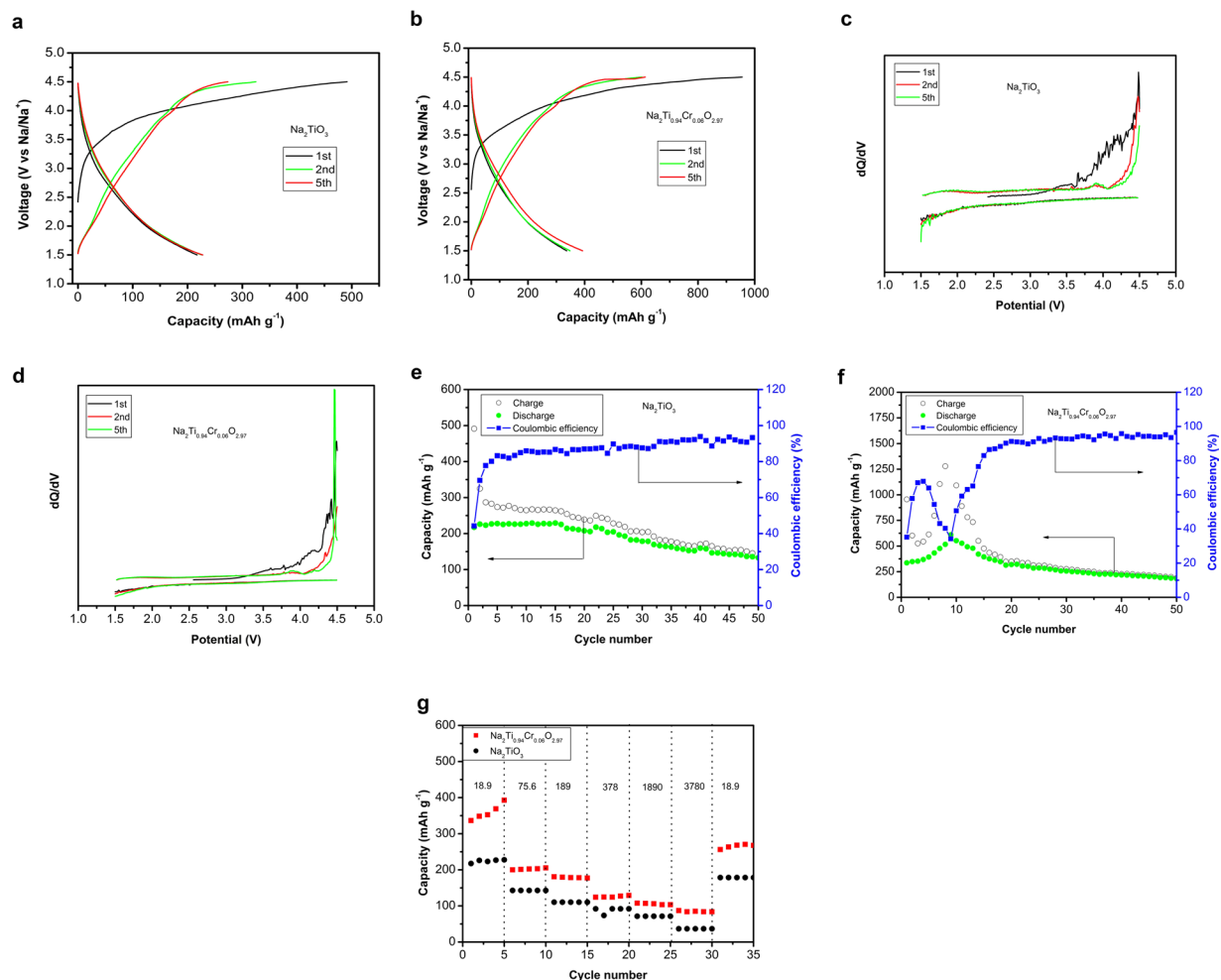


**Figure 2.** Electrochemical performances of  $\text{Na}_2\text{TiO}_3$  and  $\text{Na}_2\text{Ti}_{0.94}\text{Cr}_{0.06}\text{O}_{2.97}$ . **(a,b)** Voltage profiles of  $\text{Na}_2\text{TiO}_3$  and  $\text{Na}_2\text{Ti}_{0.94}\text{Cr}_{0.06}\text{O}_{2.97}$ . **(c,d)**  $dQ/dV$  plots of  $\text{Na}_2\text{TiO}_3$  and  $\text{Na}_2\text{Ti}_{0.94}\text{Cr}_{0.06}\text{O}_{2.97}$ . **(e,f)** Cycling performance with Coulombic efficiency of  $\text{Na}_2\text{TiO}_3$  and  $\text{Na}_2\text{Ti}_{0.94}\text{Cr}_{0.06}\text{O}_{2.97}$  at current density of  $18.9 \text{ mA g}^{-1}$ . **(g)** Rate capabilities of  $\text{Na}_2\text{TiO}_3$  and  $\text{Na}_2\text{Ti}_{0.94}\text{Cr}_{0.06}\text{O}_{2.97}$  at current density from  $18.9 \text{ mA g}^{-1}$  to  $3780 \text{ mA g}^{-1}$ .

and  $\text{Na}_2\text{Ti}_{0.94}\text{Cr}_{0.06}\text{O}_{2.97}$  are single phase and are assigned to  $\beta$  phase and monoclinic structure with a space group  $C2/c$ . The lattice parameters of  $\text{Na}_2\text{TiO}_3$  are  $13.021(0) \text{ \AA}$ ,  $13.922(0) \text{ \AA}$  and  $9.526(0) \text{ \AA}$ . The lattice parameters of  $\text{Na}_2\text{Ti}_{0.94}\text{Cr}_{0.06}\text{O}_{2.97}$  are  $12.986(4) \text{ \AA}$ ,  $13.885(0) \text{ \AA}$  and  $9.500(7) \text{ \AA}$ . It implies that small amount of addition of Cr does not change the lattice parameters significantly due to similar effective ionic radii of  $\text{Ti}^{4+}$  and  $\text{Cr}^{3+}$ .  $\text{Na}_2\text{TiO}_3$  can be reformulated as  $\text{Na}[\text{Na}_{1/3}\text{Ti}_{2/3}]\text{O}_2$  according to the Li-rich layered oxide  $\text{Li}_2\text{MnO}_3$  (ref. 20). The monoclinic cells consist of alternating Na and  $\text{Na}_{1/3}\text{Ti}_{2/3}$  layers stacked along the  $c$ -axis (Fig. 1b). Within  $\text{Na}_{1/3}\text{Ti}_{2/3}$  layers, Na cations are surrounded by six Ti cations and form a hexagon (Fig. 1c). The size of particles of  $\text{Na}_2\text{TiO}_3$  and  $\text{Na}_2\text{Ti}_{0.94}\text{Cr}_{0.06}\text{O}_{2.97}$  is about  $100 \text{ nm}$  owing to the low as-prepared temperature (Fig. 1d,e).

**Electrochemical performances of  $\text{Na}_2\text{TiO}_3$  and  $\text{Na}_2\text{Ti}_{0.94}\text{Cr}_{0.06}\text{O}_{2.97}$ .** Compared with the conventional layered sodium cathodes, the present electrode materials have several orders of magnitude lower electrical conductivities due to a lack of a transition-metal with multiple oxidation states. The low conductivities are overcome by making  $\text{Na}_2\text{TiO}_3/\text{Na}_2\text{Ti}_{0.94}\text{Cr}_{0.06}\text{O}_{2.97}$  and Super P composites via simple high energy ball milling for 5 h. We believe that the extensive research experience of carbon coating of  $\text{LiFePO}_4$  can be used with the present materials<sup>21</sup>, thus the total carbon content can be significantly decreased, and the electrode loading and energy density can be further improved. The electrochemical performances of  $\text{Na}_2\text{TiO}_3$  and  $\text{Na}_2\text{Ti}_{0.94}\text{Cr}_{0.06}\text{O}_{2.97}$  are compared as shown in Fig. 2. One interesting phenomenon is that a long potential plateau can be observed at the end of first sodium extraction in voltage profile (Fig. 2a,b), which is a common feature for all the Li-rich layered cathodes<sup>22</sup>.  $\text{Na}_2\text{TiO}_3$  delivers an initial discharge capacity of  $\sim 217 \text{ mAh g}^{-1}$  in the voltage window of  $1.5\text{--}4.5 \text{ V}$  (versus  $\text{Na}/\text{Na}^+$ ) at a current density of  $18.9 \text{ mA g}^{-1}$  (Fig. 2a).  $\text{Na}_2\text{Ti}_{0.94}\text{Cr}_{0.06}\text{O}_{2.97}$  delivers a much higher initial capacity of  $\sim 336 \text{ mAh g}^{-1}$  (Fig. 2b).

The  $dQ/dV$  plots of 1<sup>st</sup>, 2<sup>nd</sup> and 5<sup>th</sup> cycles for both  $\text{Na}_2\text{TiO}_3$  and  $\text{Na}_2\text{Ti}_{0.94}\text{Cr}_{0.06}\text{O}_{2.97}$  are plotted in Fig. 2c,d. Both samples are similar. There are no pronounced peaks on  $dQ/dV$  plots, implying no distinct charge-discharge

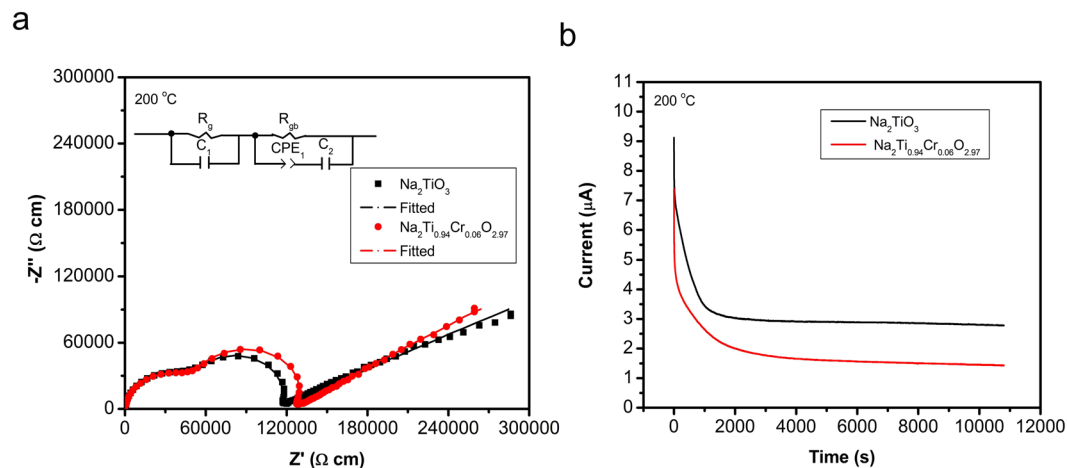


**Figure 3.** Conductivities of  $\text{Na}_2\text{TiO}_3$  and  $\text{Na}_2\text{Ti}_{0.94}\text{Cr}_{0.06}\text{O}_{2.97}$  measured in air at 200 °C. **(a)** AC impedance plots  $\bullet$ : Experimental values. The solid line represents simulated data using an equivalent circuit of  $(R_g C_1)(R_{gb} CPE_1 C_2)$  (where  $R_g$  and  $R_{gb}$  are the resistances of grain and grain-boundary respectively, CPE is the constant phase element, C is the capacitor). **(b)** DC polarization measurement at constant voltage of 1 V using Ag blocking electrodes.

plateau. The reasons are due possibly to the electrochemical inactivity of  $\text{Ti}^{4+}$  and sluggish Na-ion diffusion in  $\text{Na}_2\text{TiO}_3$  and  $\text{Na}_2\text{Ti}_{0.94}\text{Cr}_{0.06}\text{O}_{2.97}$ .

Another interesting phenomenon is that the activation processes are observed for both  $\text{Na}_2\text{TiO}_3$  and  $\text{Na}_2\text{Ti}_{0.94}\text{Cr}_{0.06}\text{O}_{2.97}$ , especially for  $\text{Na}_2\text{Ti}_{0.94}\text{Cr}_{0.06}\text{O}_{2.97}$ , in which the discharge capacity is raised to a maximum value over initial several cycles (Fig. 2e,f). As seen in Fig. 2e, the discharge capacity of  $\text{Na}_2\text{TiO}_3$  increases mildly from  $\sim 217 \text{ mAh g}^{-1}$  to  $229 \text{ mAh g}^{-1}$  over initial 15 cycles. The initial Coulombic efficiency of  $\text{Na}_2\text{TiO}_3$  is only  $\sim 44\%$  and raises to 80% after initial 4 cycles. As seen in Fig. 2f, the discharge capacity of  $\text{Na}_2\text{Ti}_{0.94}\text{Cr}_{0.06}\text{O}_{2.97}$  is much higher than that of  $\text{Na}_2\text{TiO}_3$ . The activation process is much more pronounced in that the capacity of  $\text{Na}_2\text{Ti}_{0.94}\text{Cr}_{0.06}\text{O}_{2.97}$  raises from  $\sim 336 \text{ mAh g}^{-1}$  to  $\sim 609 \text{ mAh g}^{-1}$  over initial 9 galvanostatic cycles; after that, the capacity decays mildly to  $\sim 182 \text{ mAh g}^{-1}$  after 50 galvanostatic cycles. The initial Coulombic efficiency of  $\text{Na}_2\text{Ti}_{0.94}\text{Cr}_{0.06}\text{O}_{2.97}$  is  $\sim 35\%$  and raises to 80% after initial 15 cycles. The increase in capacities over initial cycles can be attributed to the activation of the  $\text{Na}_2\text{Ti}_{0.94}\text{Cr}_{0.06}\text{O}_{2.97}$ , which is possibly related with sodium insertion to the  $\text{TiO}_2$  host structure. The decrease in capacities after full activation of  $\text{Na}_2\text{Ti}_{0.94}\text{Cr}_{0.06}\text{O}_{2.97}$  is possibly attributed to the irreversible reaction of oxygen<sup>23</sup>.

The rate capabilities of  $\text{Na}_2\text{TiO}_3$  and  $\text{Na}_2\text{Ti}_{0.94}\text{Cr}_{0.06}\text{O}_{2.97}$  are shown in Fig. 2g, the  $\text{Na}_2\text{Ti}_{0.94}\text{Cr}_{0.06}\text{O}_{2.97}$  exhibits higher capacities compared with  $\text{Na}_2\text{TiO}_3$  at different current densities. Both the materials present good capacity retention. Particularly, the capacities of  $\text{Na}_2\text{TiO}_3$  and  $\text{Na}_2\text{Ti}_{0.94}\text{Cr}_{0.06}\text{O}_{2.97}$  can be recovered to  $\sim 178$  and  $268 \text{ mAh g}^{-1}$ , ca. 82% and 80% of the initial capacities at current density of  $18.9 \text{ mA g}^{-1}$ , respectively.

**Electrical conductivities of  $\text{Na}_2\text{TiO}_3$  and  $\text{Na}_2\text{Ti}_{0.94}\text{Cr}_{0.06}\text{O}_{2.97}$ .** The electrical conductivities of  $\text{Na}_2\text{TiO}_3$  and  $\text{Na}_2\text{Ti}_{0.94}\text{Cr}_{0.06}\text{O}_{2.97}$  are evaluated by measurements of AC impedance and DC polarization at 200 °C (Fig. 3). The AC impedance plots (Fig. 3a) are simulated with an equivalent circuit of  $(R_g C_1)(R_{gb} CPE_1 C_2)$ , where  $R_g$ ,  $R_{gb}$ , C and CPE mean bulk resistance, grain-boundary resistance, capacitor element, and constant phase element, respectively. The bulk conductivity and boundary conductivity are calculated based on the two well-separated semicircles. The bulk conductivity of  $\text{Na}_2\text{Ti}_{0.94}\text{Cr}_{0.06}\text{O}_{2.97}$  ( $2.0 \times 10^{-5} \text{ S cm}^{-1}$ ) is slightly larger than that of  $\text{Na}_2\text{TiO}_3$  ( $1.7 \times 10^{-5} \text{ S cm}^{-1}$ ). The bulk conductivities of  $\text{Na}_2\text{Ti}_{0.94}\text{Cr}_{0.06}\text{O}_{2.97}$  and  $\text{Na}_2\text{TiO}_3$  are much higher than that of intrinsic conductivity of  $\text{LiFePO}_4$  ( $\sim 10^{-9} \text{ S cm}^{-1}$ )<sup>24</sup>, which implies that there is much space to improve the performance of the present materials if advanced carbon coating process is developed. The diffusion of Na cations in bulk grains would determine the redox processes in the case of active material-carbon composites. The possible creation of oxygen vacancies in  $\text{Na}_2\text{Ti}_{0.94}\text{Cr}_{0.06}\text{O}_{2.97}$  would weaken the binding of oxygen anions to migrating Na cations, thus favoring the migration of sodium ions in bulk and leading to higher bulk conductivity and better sodium deintercalation/intercalation performance. The electron conductivities are evaluated by DC polarization at 200 °C and with a constant voltage of 1 V using Ag blocking electrodes (Fig. 3b). The electron conductivities of  $\text{Na}_2\text{TiO}_3$  and  $\text{Na}_2\text{Ti}_{0.94}\text{Cr}_{0.06}\text{O}_{2.97}$  are calculated to be  $1.7 \times 10^{-6} \text{ S cm}^{-1}$  and  $0.97 \times 10^{-6} \text{ S cm}^{-1}$  based on the used voltage and steady-state current, respectively. The transference numbers of sodium ions of  $\text{Na}_2\text{TiO}_3$  and  $\text{Na}_2\text{Ti}_{0.94}\text{Cr}_{0.06}\text{O}_{2.97}$  are calculated to be  $\sim 0.81$  and 0.88, respectively, by means of (total conductivity-electron conductivity)/total conductivity, which demonstrates that the present materials are mixed ions and electrons conductive; this is advantageous for electrode materials.

**Cycling capability of  $\text{Na}_2\text{Ti}_{0.94}\text{Cr}_{0.06}\text{O}_{2.97}$ .** The long-term cycling of  $\text{Na}_2\text{Ti}_{0.94}\text{Cr}_{0.06}\text{O}_{2.97}$  is performed at current density of  $378 \text{ mA g}^{-1}$  as shown in Fig. 4. The initial discharge capacity is  $\sim 124 \text{ mAh g}^{-1}$ , and raises to  $\sim 136 \text{ mAh g}^{-1}$  after 15 cycles. The initial Coulombic efficiency is 74%, and is above 90% after initial 10 cycles. The reversible capacity is still  $100 \text{ mAh g}^{-1}$  after 1000 cycles, delivering a very low capacity decay rate of 0.026% per

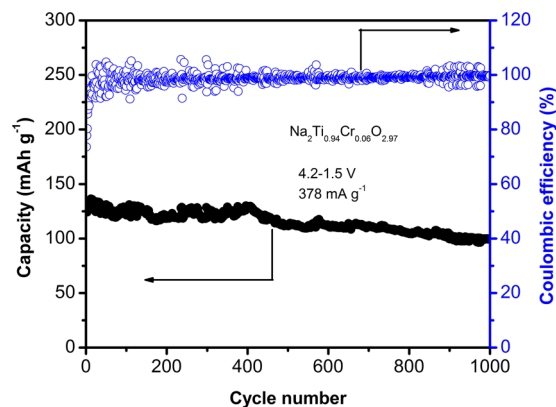


**Figure 4.** Long-term cycling of  $\text{Na}_2\text{Ti}_{0.94}\text{Cr}_{0.06}\text{O}_{2.97}$  at current density of  $378 \text{ mA g}^{-1}$ .

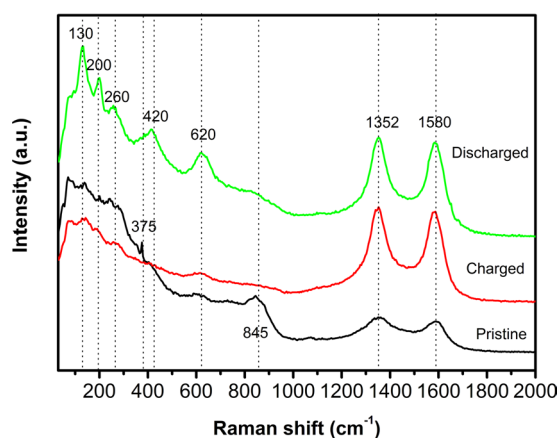


**Figure 5.** Raman spectra of pristine, charged and discharged  $\text{Na}_2\text{Ti}_{0.94}\text{Cr}_{0.06}\text{O}_{2.97}$ .

cycle, and a capacity retention of 74%, which demonstrates promising cycling capability of the material. It is noted that the present materials exhibit capacity decay with a charging voltage of 4.5 V, but good long-term cycling capability as the charging voltage decreases to 4.2 V. This implies that the capacity decay is related to the high voltage which is observed by another Na-rich layered oxide  $\text{Na}_2\text{Ru}_{0.75}\text{Sn}_{0.25}\text{O}_3$  (ref. 25).

**Raman spectroscopy.** Raman spectroscopy has been employed to evaluate the structural evolution of  $\text{Na}_2\text{Ti}_{0.94}\text{Cr}_{0.06}\text{O}_{2.97}$  upon desodiation and sodiation. The obtained Raman spectra are shown in Fig. 5. Bands at  $1352$  and  $1580 \text{ cm}^{-1}$  correspond to the D and G modes of Super P<sup>26</sup>. Thanks to Bamberger and Begun's pioneer work on Raman spectra for  $\alpha$ -,  $\beta$ - and  $\gamma$ - $\text{Na}_2\text{TiO}_3$  (ref. 19), we can characterize the structural evolution of  $\text{Na}_2\text{Ti}_{0.94}\text{Cr}_{0.06}\text{O}_{2.97}$  using Raman spectra. Two peaks around  $845 \text{ cm}^{-1}$  and one sharp peak at  $375 \text{ cm}^{-1}$  for the pristine sample can be characterized to  $\beta$  phase. Two distinct peaks at  $260$  and  $130 \text{ cm}^{-1}$  for the discharged sample also can be characterized to  $\beta$  phase, while three pronounced Raman peaks at  $620$ ,  $420$  and  $200 \text{ cm}^{-1}$  for the discharged sample can be characterized to  $\gamma$  phase. Therefore, it is indicated that ball-milled  $\text{Na}_2\text{Ti}_{0.94}\text{Cr}_{0.06}\text{O}_{2.97}$  is mainly  $\beta$  phase and with minor  $\gamma$  phase, while  $\gamma$  phase is the major phase and  $\beta$  phase is the minor phase after discharge. The Raman spectrum of charged  $\text{Na}_2\text{Ti}_{0.94}\text{Cr}_{0.06}\text{O}_{2.97}$  is poorly resolved and broad, implying that the charging process leads to certain degree of amorphization and disorder which is in agreement with the Density Functional Calculations. On the other hand, the discharged sample shows sharp Raman peaks compared with those of pristine and charged samples, indicating that better crystallization of monoclinic phase.

**XPS.** As shown in Fig. 6a, the X-ray diffraction peaks for  $\text{Na}_2\text{Ti}_{0.94}\text{Cr}_{0.06}\text{O}_{2.97}$ -carbon composite are very weak after high energy ball milling for 5 h. The composite electrodes are fully charged, which corresponds to extraction of two moles of Na, and subsequently discharged to 1.5 V. The charged and discharged samples display diffraction peak around  $44^\circ$ , which can be attributed to monoclinic  $\gamma$  phase. XPS spectra are applied to examine the change in the surface of the  $\text{Na}_2\text{Ti}_{0.94}\text{Cr}_{0.06}\text{O}_{2.97}$  electrode during desodiation/sodiation. The Cr 2p peaks are around  $577 \text{ eV}$  which can be assigned to  $\text{Cr}^{3+}$  component, though the Cr 2p spectra are poorly resolved (Fig. 6b). Figure 6c shows the Na 1s spectrum. The signal is stable at  $\sim 1071.5 \text{ eV}$  upon desodiation/sodiation, indicating the valence state of sodium cations ( $\text{Na}^{1+}$ ) is not affected during desodiation/sodiation process<sup>27</sup>. Two strong signals at  $\sim 458.3 \text{ eV}$  and  $464.1 \text{ eV}$  for the present material are ascribed to Ti  $2p_{3/2}$  and Ti  $2p_{1/2}$ , respectively

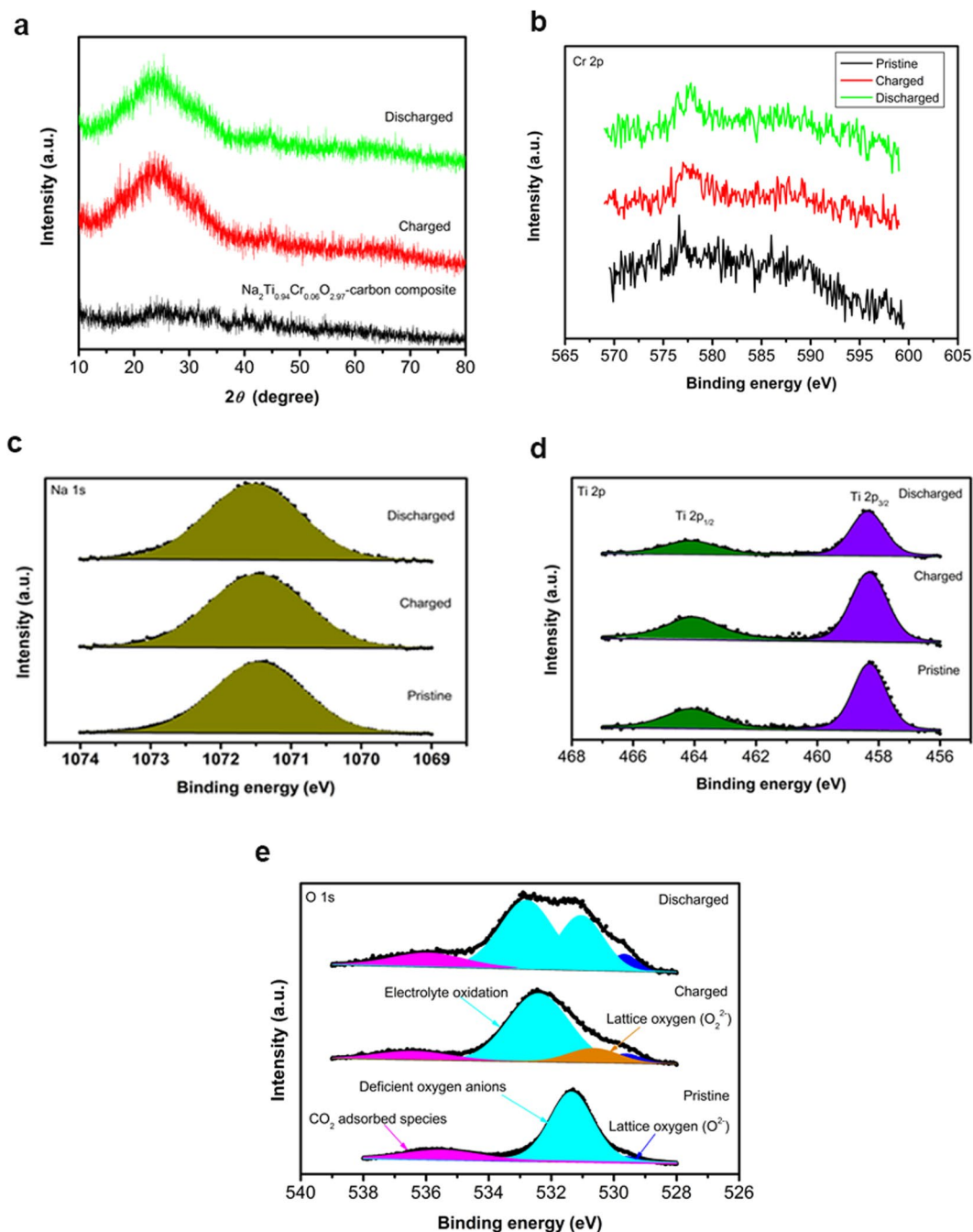


**Figure 6.** Analysis of the electrochemical desodiation and sodiation of  $\text{Na}_2\text{Ti}_{0.94}\text{Cr}_{0.06}\text{O}_{2.97}$ . **(a)** XRD patterns for the  $\text{Na}_2\text{Ti}_{0.94}\text{Cr}_{0.06}\text{O}_{2.97}$ -carbon composite, pristine electrode, fully charged sample, and discharged to 1.5 V under a current density of  $18.9 \text{ mA g}^{-1}$ . XPS spectra of the  $\text{Na}_2\text{Ti}_{0.94}\text{Cr}_{0.06}\text{O}_{2.97}$  electrodes, the spectra collected for pristine sample, fully charged sample and discharged to 1.5 V as well as by least-squares-fits using a software of XPSPEAK41. **(b)** Cr 2p spectra. **(c)** Na 1s spectra. **(d)** Ti 2p spectra. **(e)** O 1s spectra.

(Fig. 6d), corresponding to  $\text{Ti}^{4+}$  according to the ref. 28. No other Ti chemical states are detected, indicating  $\text{Ti}^{4+}$  is electrochemical inactive in the present material. Huang *et al.* also reported  $\text{Ti}^{4+}$  was electrochemical inactive<sup>29</sup>. For the O 1s spectrum of pristine  $\text{Na}_2\text{Ti}_{0.94}\text{Cr}_{0.06}\text{O}_{2.97}$  (Fig. 6e), three main components are detected, one is an oxide ion ( $\text{O}^{2-}$ ) in the crystal lattice at 529.6 eV, the peak at 535.5 eV assigns the adsorbed species<sup>22,30</sup>. The third peak at 531.4 eV may be assigned to NaOH and/or  $\text{Na}_2\text{O}_2$ , and is more probably due to oxygen anions of  $\text{Na}_2\text{Ti}_{0.94}\text{Cr}_{0.06}\text{O}_{2.97}$  in the subsurface (bulk structure near the surface), which have a deficient coordination number<sup>30–32</sup>. The spectrum mildly changes when the sample is fully charged, the component at 532.4 eV is C = O bonds in polycarbonates, implying the decomposition of electrolyte solvents<sup>33,34</sup>. The decomposition of polycarbonates is irreversible upon discharging, where the peak around 532–533 eV is remained. A new component at 530.6 eV corresponds to oxide ions with lower electronic density compared with  $\text{O}^{2-}$ , namely  $\text{O}_2^{2-}$  species<sup>30,35</sup>.

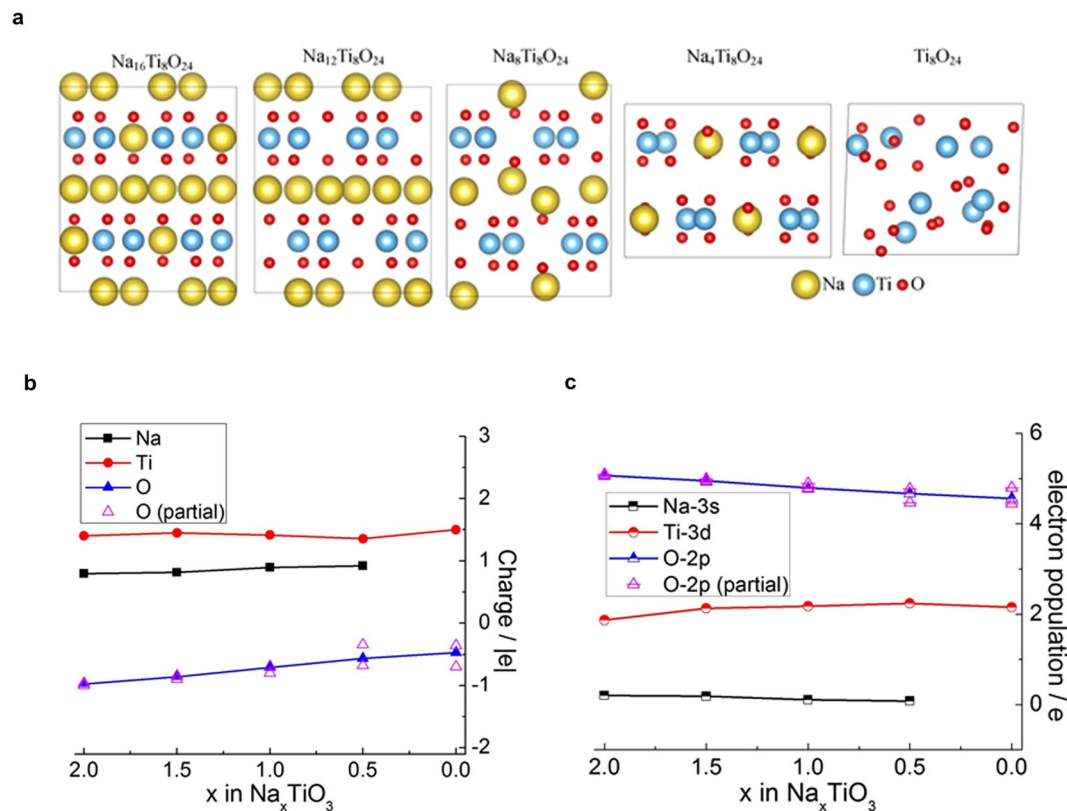


**Figure 7.** Density Functional Calculations for Na<sub>2</sub>TiO<sub>3</sub>. **(a)** Optimized structures of Na<sub>16</sub>Ti<sub>8</sub>O<sub>24</sub>, Na<sub>12</sub>Ti<sub>8</sub>O<sub>24</sub>, Na<sub>8</sub>Ti<sub>8</sub>O<sub>24</sub>, Na<sub>4</sub>Ti<sub>8</sub>O<sub>24</sub> and Ti<sub>8</sub>O<sub>24</sub> from left to right. **(b)** Mulliken and **(c)** Electron populations of the valence orbital of each element in Na<sub>16</sub>Ti<sub>8</sub>O<sub>24</sub>, Na<sub>12</sub>Ti<sub>8</sub>O<sub>24</sub>, Na<sub>8</sub>Ti<sub>8</sub>O<sub>24</sub>, Na<sub>4</sub>Ti<sub>8</sub>O<sub>24</sub> and Ti<sub>8</sub>O<sub>24</sub> which corresponds x = 2, 1.5, 1, 0.5, 0 in Na<sub>x</sub>TiO<sub>3</sub> respectively. The lines connect average populations of each orbitals in different concentrations. The magenta triangles show average populations of 2p orbitals of different types of oxygen atoms at each concentration.

It is suggested that the lattice oxygen O<sup>2-</sup> transforms partially to O<sub>2</sub><sup>2-</sup> upon the desodiation process. After the sodiation, the O<sub>2</sub><sup>2-</sup> component disappears, while the defective oxygen component partly remains. These phenomena demonstrate that the redox reactivity of oxygen is involved in the electrochemical desodiation and sodiation processes. We can quasi-quantificationally analyze the Na/Ti ratio from the XPS using the peak area and relative sensitivity factor (RSF) of element. Na/Ti ratio = [Area (Na)/RSF(Na)]/[Area (Ti)/RSF(Ti)]. It implies probably Na extraction upon charging and returning upon discharging (Table S1).

**Density Functional Calculations.** The participation of the oxygen redox is also confirmed by ab initio calculations. The computed crystalline structures of Na<sub>16</sub>Ti<sub>8</sub>O<sub>24</sub>, Na<sub>12</sub>Ti<sub>8</sub>O<sub>24</sub>, Na<sub>8</sub>Ti<sub>8</sub>O<sub>24</sub>, Na<sub>4</sub>Ti<sub>8</sub>O<sub>24</sub> and Ti<sub>8</sub>O<sub>24</sub> are shown in Fig. 7a. With the number of Na atoms in the cell decreasing, the structure eventually becomes disordered which corresponds to the instability of TiO<sub>3</sub>.

Mulliken charges of each element in Na<sub>16</sub>Ti<sub>8</sub>O<sub>24</sub>, Na<sub>12</sub>Ti<sub>8</sub>O<sub>24</sub>, Na<sub>8</sub>Ti<sub>8</sub>O<sub>24</sub>, Na<sub>4</sub>Ti<sub>8</sub>O<sub>24</sub> and Ti<sub>8</sub>O<sub>24</sub> are plotted in Fig. 7b. The Na atoms are ionized. With the increase of number of Na atoms in the cell, the charge of O increases (becomes more negative) while the charge of Ti is relatively stable. This indicates charge transfer from Na to O. There are two types of O atoms in this material: one is coordinated to Na and the other is coordinated only to Ti which have different Mulliken populations as shown by empty triangles in Fig. 7b. The full sodiation corresponds to the same charge balance as in the stoichiometric TiO<sub>2</sub> with all oxygens in the O<sup>2-</sup> states and the triangles in Fig. 7b coincide. As the material is desodiated, the charge difference between the two types of O increases. This is due to the valence electrons of Na occupying the 2p orbitals of O atoms which are coordinated to Na. During desodiation, the population of the 2p orbitals of these O atoms decreases, as the electrons leave the material together with Na ions, and the overall negative charge of these oxygen atom decreases as can be seen in Fig. 7c. We note that the absolute magnitudes of the charges are not equal to the assumed redox states (Ti<sup>4+</sup>, O<sup>2-</sup>) due to the use of Mulliken analysis with localized basis functions, as expected.

## Discussion

Among layered sodium oxides, P2-type Na<sub>2/3</sub>Fe<sub>1/2</sub>Mn<sub>1/2</sub>O<sub>2</sub> (ref. 9), α-NaMnO<sub>2</sub> (ref. 10), β-NaMnO<sub>2</sub> (ref. 11), P2-type Na<sub>0.67</sub>Mn<sub>0.8</sub>Mg<sub>0.2</sub>O<sub>2</sub> (ref. 12), and so on had been reported to deliver high discharge capacities of 150~190 mAh g<sup>-1</sup>, with the theoretical capacities of 264 mAh g<sup>-1</sup>, 244 mAh g<sup>-1</sup>, and 227 mAh g<sup>-1</sup>, respectively. Among typical polyanion compounds, NASICON-type Na<sub>3</sub>V<sub>2</sub>(PO<sub>4</sub>)<sub>3</sub> (ref. 15), maricite-type NaFePO<sub>4</sub> (ref. 16),

$\text{Na}_{3.12}\text{Fe}_{2.44}(\text{P}_2\text{O}_7)_2$  (ref. 17), and so on had reversible capacities of  $114 \text{ mAh g}^{-1}$ ,  $142 \text{ mAh g}^{-1}$  and  $85 \text{ mAh g}^{-1}$ , with the theoretical capacities of  $118 \text{ mAh g}^{-1}$ ,  $155 \text{ mAh g}^{-1}$ , and  $118 \text{ mAh g}^{-1}$ , respectively. To the best of our knowledge, the present material benchmarks the highest-ever capacity by far discovered among other known sodium cathode materials. The high capacities are possibly related with the redox reaction of oxygen as demonstrated by XPS and Density Functional Calculations.

Besides high reversible capacities, the present  $\text{Na}_2\text{Ti}_{0.94}\text{Cr}_{0.06}\text{O}_{2.97}$  exhibits promising cycling capability with capacity retention of 74% after 1000 cycles. The conventional layered sodium oxides have limited cycling capability because of a possibility of multiple phase transitions during cycling, i.e. a structural instability<sup>36</sup>, which is facilitated by a large ionic radius of Na. The as-prepared  $\text{Na}_2\text{Ti}_{0.94}\text{Cr}_{0.06}\text{O}_{2.97}$  possess  $\beta$  phase and monoclinic Na-rich layered structure, which is transformed to mixed phases of  $\beta$  and  $\gamma$  upon discharging. Both  $\beta$  and  $\gamma$  phases possess monoclinic structures, which contributing the promising cycling capability.

In summary, we for the first time have investigated Na-rich layered compound  $\text{Na}_2\text{TiO}_3$  as a new cathode for the Na-ion batteries. We find that  $\text{Na}_2\text{TiO}_3$  cathode has a high reversible capacity of  $\sim 217 \text{ mAh g}^{-1}$ . Carbon coating had to be used to overcome its low conductivity. By doping  $\text{Na}_2\text{TiO}_3$  with  $\text{Cr}^{3+}$  to create oxygen vacancies and to facilitate the migration of Na-ions, we achieve a much higher reversible capacity of  $\sim 336 \text{ mAh g}^{-1}$ . Furthermore, we demonstrate that the new Na-rich layered cathode Cr-doped  $\text{Na}_2\text{TiO}_3$  shows long-term cycling capability (74% capacity retention after 1000 cycles, a very low capacity decay rate of 0.026% per cycle), which is superior to most mainstream layered sodium cathodes. A challenge for future work is to reduce the concentration of carbon and to improve the conductivity. We strongly believe that the present work will not only open up a viable strategy for designing and discovering new sodium cathodes, but also inspire future success in exploring superior electrode materials for next-generation rechargeable batteries.

## Methods

**Materials synthesis.** To synthesize the  $\text{Na}_2\text{TiO}_3$ , proper amounts of  $\text{TiO}_2$  (Sigma-Aldrich, 99.9%) and NaOH (Sigma-Aldrich, 10% excess) were milled for 4 h. The mixture was then heated in alumina crucibles at  $500^\circ\text{C}$  for 6 h under atmosphere of air. To synthesize  $\text{Na}_2\text{Ti}_{0.94}\text{Cr}_{0.06}\text{O}_{2.97}$ ,  $\text{TiO}_2$ - $\text{Cr}_2\text{O}_3$  solid solution was first synthesized by mixing  $\text{TiO}_2$  and  $\text{Cr}_2\text{O}_3$  (Sigma-Aldrich) for at least 24 h followed by high-energy ball-milling for 5 h (SPEX SamplePrep 8000 M Mixer), then homogenized with 10% excess of NaOH and annealed at  $500^\circ\text{C}$  for 6 h under air atmosphere. To prepare the electrode-carbon composite,  $\text{Na}_2\text{TiO}_3$  or  $\text{Na}_2\text{Ti}_{0.94}\text{Cr}_{0.06}\text{O}_{2.97}$  was mixed with Super P (TIMCAL Ltd.) in a weight ratio of 1: 1 and was milling under Ar atmosphere for 5 h (SPEX SamplePrep 8000 M Mixer).

**XRD and SEM.** The XRD measurements were performed in a  $2\theta$  range of  $10$ – $70^\circ$  using Shimadzu XRD-6000 Cu-K $\alpha$ . The microstructure of powdered materials was examined using SEM (S-4300 Shimadzu).

**Conductivity.** The bulk conductivity measurements were evaluated by AC impedance spectroscopy (Solartron 1260/1287) at  $200^\circ\text{C}$ , with applying potential of 10 mV from 32 MHz to 1 Hz. The  $\text{Na}_2\text{TiO}_3$  and  $\text{Na}_2\text{Ti}_{0.94}\text{Cr}_{0.06}\text{O}_{2.97}$  powders were pelletized and sintered at  $550^\circ\text{C}$  for 6 h under air atmosphere. Conductive Ag paste was coated on two sides of the pellets to form ion-blocking electrodes. To perform DC measurements, conductive Ag paint ( $>1000 \text{ S cm}^{-1}$ ) was coated on two sides of the  $\text{Na}_2\text{TiO}_3$  and  $\text{Na}_2\text{Ti}_{0.94}\text{Cr}_{0.06}\text{O}_{2.97}$  pellets, and dried at  $120^\circ\text{C}$  for 5 min. A constant voltage of 1 V is applied after the coated pellets were held for 1 h at  $200^\circ\text{C}$  under air atmosphere, and variation of DC current was monitored until steady-state current was obtained.

**Electrochemical characterization.** The battery performance was tested using 2016-type coin cell on MACCOR and LAND battery cycler instruments. The working electrode was prepared by mixing 80 wt%  $\text{Na}_2\text{TiO}_3/\text{Na}_2\text{Ti}_{0.94}\text{Cr}_{0.06}\text{O}_{2.97}$ -carbon active material, 10 wt% polyvinylidene fluoride (PVDF, Sigma), and 10 wt% Super P (TIMCAL Ltd.) in N-methylpyrrolidone (NMP, Sigma) solvent for at least 12 h. The electrode slurry was coated on aluminum foils and dried at  $120^\circ\text{C}$  in vacuum for at least 12 h, with an average active material loading of  $\sim 0.6 \text{ mg cm}^{-2}$ . The electrolyte is 1 M  $\text{NaClO}_4$  in ethylene carbonate (EC)/propylene carbonate (PC) (1:1 in weight). The glass microfiber filter (Whatman, GF/A) was dried at  $50^\circ\text{C}$  in vacuum for 48 h and was used as separator. The 2016-type coin cell was assembled with working electrode, electrolyte, separator, and metallic sodium (Sigma, 99.99%) in Ar-filled glove box. The galvanostatic charge and discharge measurements were conducted in the voltage window of 4.5–1.5 V and 4.2–1.5 V at different current densities from 18.9 mA  $\text{g}^{-1}$  to 3780 mA  $\text{g}^{-1}$ .

**Raman.** Raman spectra were recorded with Horiba Jobin Yvon Modular Raman Spectrometer using 514 nm Stellar Pro Argon-ion laser. The system was calibrated using a silicon reference before the measurement ( $520.5 \text{ cm}^{-1}$ ). The mixture of  $\text{Na}_2\text{Ti}_{0.94}\text{Cr}_{0.06}\text{O}_{2.97}$  and Super P with ball milling 5 h is as pristine sample. For the first-cycled charged and discharged samples, the cells were fully charged and discharged to 1.5 V, then were decomposed. The electrode pellets were directly conducted on Raman.

**XPS.** XPS measurement was performed using Kratos AXIS Ultra<sup>DLD</sup> spectrometer applying a monochromated Al K $\alpha$  X-ray source (1486.71 eV photons) and a dwelling time of 100 ms. The binding energy of the spectra was calibrated against C 1 s peak at 285 eV. The XPS spectra were mathematically fitted using XPSPEAK41 software. Core peaks were analysed using a Linear-type background. For XPS measurement of pristine sample, the as-prepared  $\text{Na}_2\text{Ti}_{0.94}\text{Cr}_{0.06}\text{O}_{2.97}$  powder was stucked on the sample hold of the XPS spectrometer. For the XPS measurements of charge-discharge electrodes, the charged and discharged electrodes were stripped from the Al foils and dried in glove box and were stucked on the sample hold of the XPS spectrometer in air, and were performed XPS measurements immediately to avoid exposing longly to air.

**Density Functional Calculations.** Density Functional Theory (DFT) was used to optimize crystalline structures with the SIESTA code<sup>37</sup>. The PBE exchange-correlation functional and a DZP (double- $\zeta$  polarized) basis set were used<sup>38</sup>. Spin polarization was checked and found to be unimportant. A TZP (triple- $\zeta$  polarized) basis was tested and did not significantly change the results vs. DZP. The basis set for Na was optimized to reproduce the cohesive energies of Na. For other elements, the basis set was generated with the setting “PAO. EnergyShift = 0.002 Ry”. Geometries were optimized until forces on all atoms were below 0.02 eV/Å and pressure was below 0.1 GPa. A cutoff of 200 Ry was used for the Fourier expansion of the density. An electronic temperature of 1000 K was used to facilitate convergence. The Brillouin zone was sampled with a  $5 \times 3 \times 3$  grid of Monkhorst-Pack points<sup>39</sup>. The initial lattice parameters of the unit cell are  $a = 5.37$  Å,  $b = 9.31$  Å and  $c = 11.07$  Å;  $\alpha = 90.00^\circ$ ,  $\beta = 99.68^\circ$  and  $\gamma = 90.00^\circ$  for  $\text{Na}_{16}\text{Ti}_8\text{O}_{24}$ , which is taken from the Material Project with ID of mp-752423<sup>40</sup>. The optimized  $\text{Na}_{16}\text{Ti}_8\text{O}_{24}$  shows lattice parameters about:  $a = 5.39$  Å,  $b = 9.36$  Å and  $c = 11.02$  Å;  $\alpha = 90.00^\circ$ ,  $\beta = 99.70^\circ$  and  $\gamma = 90.00^\circ$ , which are in good agreement with the initial ones. The trend of charges of each element on the number of Na atoms in the formula was analyzed qualitatively by using Mulliken charges.

## References

1. Tarascon, J.-M. Is lithium the new gold. *Nature Chem* **2**, 510 (2010).
2. Yabuuchi, N., Kubota, K., Dahbi, M. & Komaba, S. Research development on sodium-ion batteries. *Chem. Rev.* **114**, 11636–11682 (2014).
3. Dunn, B., Kamath, H. & Tarascon, J.-M. Electrical energy storage for the grid: a battery of choices. *Science* **334**, 928–934 (2011).
4. Kim, S., Seo, D., Ma, X., Ceder, G. & Kang, K. Electrode materials for rechargeable sodium-ion batteries: potential alternatives to current lithium-ion batteries. *Adv. Energy Mater* **2**, 710–721 (2012).
5. Delmas, C., Fouassier, C. & Hagemuller, P. Structural classification and properties of the layered oxides. *Physica B + C* **99**, 81–85 (1980).
6. Zhao, J., Zhao, L., Dimov, N., Okada, S. & Nishida, T. Electrochemical and thermal properties of  $\alpha$ - $\text{NaFeO}_2$  cathode for Na-ion batteries. *J. Electrochem. Soc.* **160**, A3077–A3081 (2013).
7. Yu, C. Y. *et al.*  $\text{NaCrO}_2$  cathode for high-rate sodium-ion batteries. *Energy Environ. Sci.* **8**, 2019–2026 (2015).
8. Han, M. H., Gonzalo, E., Casas-Cabanas, M. & Rojo, T. Structural evolution and electrochemistry of monoclinic  $\text{NaNiO}_2$  upon the first cycling process. *J. Power Sources* **258**, 266–271 (2014).
9. Yabuuchi, N. *et al.* P2-type  $\text{Na}_x[\text{Fe}_{1/2}\text{Mn}_{1/2}]\text{O}_2$  made from earth-abundant elements for rechargeable Na batteries. *Nat. Mater.* **11**, 512–517 (2012).
10. Ma, X. H., Chen, H. L. & Ceder, G. Electrochemical properties of monoclinic  $\text{NaMnO}_2$ . *J. Electrochem. Soc.* **158**, A1307–A1312 (2011).
11. Billaud, J. *et al.* Beta- $\text{NaMnO}_2$ : a high-performance cathode for sodium-ion batteries. *J. Am. Chem. Soc.* **136**, 17243–17248 (2014).
12. Billaud, J. *et al.*  $\text{Na}_{0.67}\text{Mn}_{1-x}\text{Mg}_x\text{O}_2$  ( $0 \leq x \leq 0.2$ ): a high capacity cathode for sodium-ion batteries. *Energy Environ. Sci.* **7**, 1387–1391 (2014).
13. Lee, E. *et al.* Layered P2/O3 intergrowth cathode: toward high power Na-ion batteries. *Adv. Energy Mater* **4**, 1400458 (2014).
14. Guo, S. H. *et al.* A layered P2- and O3-type composite as a high-energy cathode for rechargeable sodium-ion batteries. *Angew. Chem. Int. Ed.* **54**, 5894–5899 (2015).
15. Jiang, Y. *et al.* Nanoconfined carbon-coated  $\text{Na}_3\text{V}_2(\text{PO}_4)_3$  particles in mesoporous carbon enabling ultralong cycle life for sodium-ion batteries. *Adv. Energy Mater* **5**, 1402104 (2015).
16. Kim, J. *et al.* Unexpected discovery of low-cost maricite  $\text{NaFePO}_4$  as a high-performance electrode for Na-ion batteries. *Energy Environ. Sci.* **8**, 540–545 (2015).
17. Ha, K. *et al.*  $\text{Na}_{4-\alpha}\text{M}_{2+\alpha/2}(\text{P}_2\text{O}_7)_2$  ( $2/3 \leq \alpha \leq 7/8$ ,  $M = \text{Fe}, \text{Fe}_{0.5}\text{Mn}_{0.5}, \text{Mn}$ ): A promising sodium ion cathode for Na-ion batteries. *Adv. Energy Mater* **3**, 770–776 (2013).
18. Hill, W. A. & Moon, A. R. Alkali oxide rich sodium titanates. *J. Am. Ceram. Soc.* **68**, C266–C267 (1985).
19. Bamberger, C. E. & Begun, G. M. Sodium titanates: stoichiometry and Raman spectra. *J. Am. Ceram. Soc.* **70**, C48–C51 (1987).
20. Thackeray, M. M. *et al.*  $\text{Li}_2\text{MnO}_3$ -stabilized  $\text{LiMO}_2$  ( $M = \text{Mn}, \text{Ni}, \text{Co}$ ) electrodes for lithium-ion batteries. *J. Mater. Chem.* **17**, 3112–3125 (2007).
21. Doeff, M. M., Hu, Y., McLarnon, F. & Kostecki, R. Effect of surface carbon structure on the electrochemical performance of  $\text{LiFePO}_4$ . *Electrochem. Solid-State Lett* **6**, A207–A209 (2003).
22. Rajarathinam, S., Mitra, S. & Petla, R. K.  $\text{Li}_2\text{MnO}_3$  rich- $\text{LiMn}_{0.33}\text{Co}_{0.33}\text{Ni}_{0.33}\text{O}_2$  integrated nano-composites as high energy density lithium-ion battery cathode materials. *Electrochim. Acta* **108**, 135–144 (2013).
23. Yabuuchi, N., Yoshii, K., Myung, S.-T., Nakai, I. & Komaba, S. Detailed studies of a high-capacity electrode material for rechargeable batteries,  $\text{Li}_2\text{MnO}_3$ - $\text{LiCo}_{1/3}\text{Ni}_{1/3}\text{Mn}_{1/3}\text{O}_2$ . *J. Am. Chem. Soc.* **133**, 4404–4419 (2011).
24. Xu, Y. *et al.* Electronic structure and electrical conductivity of undoped  $\text{LiFePO}_4$ . *Electrochem. Solid-State Lett* **7**, A131–A134 (2004).
25. Rozier, P. *et al.* Anionic redox chemistry in Na-rich  $\text{Na}_2\text{Ru}_{1-y}\text{Sn}_y\text{O}_3$  positive electrode material for Na-ion batteries. *Electrochem. Commun.* **53**, 29–32 (2015).
26. Ruther, R. E. *et al.* Raman microscopy of lithium-manganese-rich transition metal oxide cathodes. *J. Electrochem. Soc.* **162**, A98–A102 (2015).
27. Shchukarev, A., Boily, J.-F. & Felmy, A. R. XPS of fast-frozen hematite colloids in NaCl aqueous solutions: I. evidence for the formation of multiple layers of hydrated sodium and chloride ions induced by the {001} basal plane. *J. Phys. Chem. C* **111**, 18307–18316 (2007).
28. Liu, C., Tang, X., Mo, C. & Qiang, Z. Characterization and activity of visible-light-driven  $\text{TiO}_2$  photocatalyst codoped with nitrogen and cerium. *J. Solid State Chem.* **181**, 913–919 (2008).
29. Wang, Y. S. *et al.* Ti-substituted tunnel-type  $\text{Na}_{0.44}\text{MnO}_2$  oxide as a negative electrode for aqueous sodium-ion batteries. *Nat. Commun.* **6**, 1–10 (2015).
30. Dupin, J. C., Gonbeau, D., Vinatier, P. & Lavesseur, A. Systematic XPS studies of metal oxides, hydroxides and peroxides. *Phys. Chem. Chem. Phys.* **2**, 1319–1324 (2000).
31. Dahéron, L. *et al.* Electron transfer mechanisms upon lithium deintercalation from  $\text{LiCoO}_2$  to  $\text{CoO}_2$  investigated by XPS. *Chem. Mater.* **20**, 583–590 (2008).
32. Okonkwo, I. A. *et al.* Oxidation states of molybdenum in oxide films formed in sulphuric acid and sodium hydroxide. *Thin Solid Films* **520**, 6318–6327 (2012).
33. Dedryvere, R. *et al.* Electrode/electrolyte interface reactivity in high-voltage spinel  $\text{LiMn}_{1.6}\text{Ni}_{0.4}\text{O}_4/\text{Li}_4\text{Ti}_5\text{O}_{12}$  lithium-ion battery. *J. Phys. Chem. C* **114**, 10999–1008 (2010).
34. Xu, M., Lu, D., Garsuch, A. & Lucht, B. L. Improved performance of  $\text{LiNi}_{0.3}\text{Mn}_{1.5}\text{O}_4$  cathodes with electrolytes containing dimethylmethylphosphonate (DMMP). *J. Electrochem. Soc.* **159**, A2130–A2134 (2012).
35. Sathiya, M. *et al.* Reversible anionic redox chemistry in high-capacity layered-oxide electrodes. *Nat. Mater.* **12**, 827–835 (2013).

36. Han, M. M., Gonzalo, E., Singh, G. & Rojo, T. A comprehensive review of sodium layered oxides: powerful cathodes for Na-ion batteries. *Energy Environ. Sci.* **8**, 81–102 (2015).
37. Kohn, W. & Sham, L. J. Self-consistent equations including exchange and correlation effects. *Phys. Rev.* **140**, A1133–A1138 (1965).
38. Perdew, J. P., Burke, K. & Ernzerhof, M. Generalized gradient approximation made simple. *Phys. Rev. Lett.* **77**, 3865–3868 (1996).
39. Monkhorst, H. J. & Pack, J. D. Special points for Brillouin-zone integrations. *Phys. Rev. B* **13**, 5188–5192 (1976).
40. *Materials Project Network* <https://www.materialsproject.org/materials/mp-752423/>.

## Acknowledgements

This research is supported by Chongqing University, the Fundamental Research Funds for the Central Universities (No. 0241005202014, No. 0903005203403), National Natural Science Foundation of China (Nos 11632004, 51572182, 11372104, 11372363, 11332013 and 5121543), the Key Program for International Science and Technology Cooperation Projects of the Ministry of Science and Technology of China (No. 2016YFE0125900), National University of Singapore, the National Research Foundation, Prime Minister's Office, Singapore under its Competitive Research Programme (CRP Award No. NRF-CRP 8-2011-04), Ministry of Education of Singapore under 2 MOE 2015-T2-1-011 grant.

## Author Contributions

S.F.S. conceived the ideas and performed the experiments. M.K. performed the electrochemical performance of  $\text{Na}_2\text{TiO}_3$  and measurement of Raman spectra. Y.Q.C. and S.M. programmed and ran the simulation and analysed the data. S.F.S., N.H. and L.L. discussed and analysed the results. S.F.S. wrote the manuscript. C.H.X. commented on the manuscript. S.M., L.L. and N.H. polished the manuscript. All authors approved the manuscript.

## Additional Information

**Supplementary information** accompanies this paper at doi:[10.1038/s41598-017-00346-x](https://doi.org/10.1038/s41598-017-00346-x)

**Competing Interests:** The authors declare that they have no competing interests.

**Publisher's note:** Springer Nature remains neutral with regard to jurisdictional claims in published maps and institutional affiliations.



This work is licensed under a Creative Commons Attribution 4.0 International License. The images or other third party material in this article are included in the article's Creative Commons license, unless indicated otherwise in the credit line; if the material is not included under the Creative Commons license, users will need to obtain permission from the license holder to reproduce the material. To view a copy of this license, visit <http://creativecommons.org/licenses/by/4.0/>

© The Author(s) 2017